

# Suppressed compressibility of quantum Hall effect edge states in epitaxial graphene on SiC

Sergey Slizovskiy\* and Vladimir I. Fal'ko

*National Graphene Institute, The University of Manchester, M13 9PL, Booth st. E., Manchester, UK*

We determine conditions for the formation of compressible stripes near the quantum Hall effect (QHE) edges of top-gated epitaxial graphene on Si-terminated SiC (G/SiC) and compare those to graphene exfoliated onto insulating substrate in the field-effect-transistor (GraFET) geometry. For G/SiC, a large density of localised surface states on SiC just underneath graphene layer and charge transfer between them lead both to doping of graphene and to screening of potential profile near its edge. This suppresses formation of compressible stripes near QHE edges in graphene, making them much narrower than the corresponding compressible stripes in GraFETs.

## I. INTRODUCTION

Edge states in the quantum Hall effect (QHE) systems<sup>1–6</sup> are chiral, providing transport channels that carry electrons along the edge in the direction set by magnetic field polarity. Over the years, investigations of the structure of edge states in semiconductor heterostructures were carried out for the understanding of current noise<sup>7–11</sup> and cooling rates<sup>12–14</sup> in the QHE regime. For electrons in GaAs/AlGaAs devices, it has been shown<sup>9,15–18</sup> that, in a strong magnetic field, an electrostatically soft edge of a 2D electron gas reconstructs into a sequence of compressible and incompressible stripes. A similar possibility was recently suggested for graphene<sup>19–23</sup>, where an essential difference arises from a  $|y|^{-1/2}$  singularity in the charge density near the edge<sup>24</sup> graphene-specific edge states<sup>25–29</sup>.

When epitaxial graphene is grown on Si-terminated face of SiC (G/SiC), a “dead layer” of carbons forms on the SiC surface, right underneath graphene<sup>30,31</sup>. This dead layer carries a large density of localised states, and charge transfer<sup>32–37</sup> between graphene and these surface states dopes graphene. At a strong magnetic field, such charge transfer pins graphene doping at integer filling factors<sup>36,37</sup>, leading to the anomalously wide QHE plateaux, in particular, at filling factors  $\nu = \pm 2$ . This makes G/SiC a promising material platform for the realisation of metrological resistance standard based on the QHE phenomenon<sup>33–42</sup>. For practical applications of G/SiC in resistance metrology, which requires achieving robust QHE plateaux at moderate magnetic fields, top gating is used to reduce graphene doping. This should be contrasted to graphene exfoliated onto an insulating substrate in a field-effect transistor (GraFET), where gates are used to dope otherwise neutral graphene. Below, we show that these features of G/SiC, as well as an efficient electrostatic screening produced by charge transfer between graphene and surface states on SiC suppress the formation of compressible stripes near graphene edge.

Here, we consider G/SiC with a top gate located at a distance  $d$  above graphene and extended beyond the edge of graphene flake, as shown in Fig. 1. We assume that, far away from the edge ( $y \rightarrow \infty$ ), graphene is tuned to the most robust  $\nu = \pm 2$  QHE plateau states. In Section

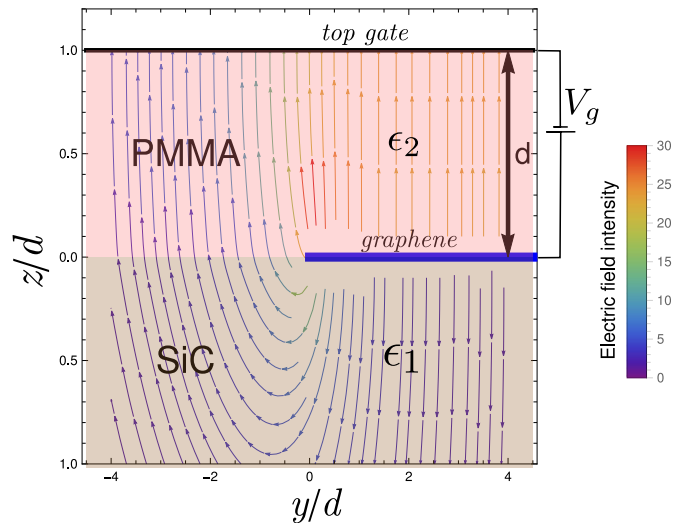


FIG. 1. Edge of gated epitaxial graphene on SiC (G/SiC). Electric field lines are plotted with color indicating the field strength. The parameters used in numerical analysis are:  $\epsilon_1 = 9.7$ ,  $\epsilon_2 = 3.5$ ,  $d = 20 \div 400$  nm.

II, we model the electrostatic environment of such gated G/SiC devices. This gives an input for analysing the self-consistent potential near the edge and for finding the electronic spectrum in quantizing magnetic fields. In Section III, we show that, when a significant potential inhomogeneity builds up, extra pairs of counter-propagating edge channels start to appear at the edge, whereas the inner edge state may give rise to a narrow compressible stripe. In Section IV, we compare the edge states in G/SiC with edge states in GraFETs, concluding that in G/SiC formation of compressible stripes is strongly suppressed by the features of charge transfer in this system.

## II. EDGE POTENTIAL PROFILE FOR GATED G/SiC

In this section we analyse the electrostatics of graphene’s edge in typical devices used in graphene QHE metrology<sup>33–36</sup>, Fig. 1, where epitaxial G/SiC is coated with PMMA and top-gated using a metallic electrode. It has been noticed<sup>30,31,43</sup> that, due to the work func-

tion difference between graphene and SiC surface states, epitaxial graphene grown on Si-terminated face of SiC (G/SiC) is significantly electron-doped by the charge transfer<sup>32-37</sup> from the dead layer of carbons on SiC surface. Based on parameters quoted in Refs.[36] and [40], we use  $\gamma \approx 2 \text{ nm}^{-2} \text{ eV}^{-1}$  for the density of localized surface states on SiC, which appear in the immediate vicinity,  $d_1 \approx 0.3 \text{ nm} \ll d$ , of graphene. To reduce the electron doping of graphene and achieve QHE filling factor  $\nu = \pm 2$  for magnetic fields range,  $B \sim 5 - 15$  Tesla, one employs electrostatic gating.

Due to the presence of donors just underneath graphene, the compressibility of electrons in this system never falls below the value determined by  $\gamma$ , even in places where the Fermi level,  $\mu$ , falls between Landau levels in graphene. Therefore, for so large  $\gamma$  that

$$\frac{\gamma e^2 d}{2\pi\epsilon_0(\epsilon_1 + \epsilon_2)} \equiv \tilde{\gamma} \gg 1,$$

the quantum capacitance of graphene together with a surface dead layer is much larger than the geometric capacitance, resulting in a metallic behaviour of this system. For G/SiC,  $\tilde{\gamma}$  falls in the range  $10 < \tilde{\gamma} < 200$  for the device parameters listed in Fig. 1, allowing us to consider graphene electrons and SiC surface donors, with a total charge density,

$$\rho(y) = -en_G(y) + en_{D+}, \quad (1)$$

as an almost perfectly screening charge system on the half-plane,  $y > 0$ ,  $z = 0$ . Imposing the condition  $\varphi(y, d) = 0$  at the metallic top gate, one finds<sup>19</sup>

$$\begin{aligned} \varphi(y, z < 0) &= \frac{1}{2\pi\epsilon_0} \int_0^\infty \left[ -\frac{2\rho(y')}{\epsilon_1 + \epsilon_2} \ln |\mathbf{R}| \right. \\ &\quad \left. + \sum_{n=1}^\infty \frac{4\epsilon_2 \rho(y') \xi^n}{\epsilon_1^2 - \epsilon_2^2} \ln |\mathbf{R} - 2nd| \right] dy', \\ \varphi(y, z > 0) &= \int_0^\infty \sum_{n=0}^\infty \frac{2\rho(y') \xi^n}{2\pi\epsilon_0(\epsilon_1 + \epsilon_2)} \ln \frac{|\mathbf{R} - 2(n+1)\mathbf{d}|}{|\mathbf{R} + 2nd|} dy'. \end{aligned} \quad (2)$$

Here  $\mathbf{R} = (0, y - y', z)$ ,  $\mathbf{d} = (0, 0, d)$  and  $\xi = \frac{\epsilon_1 - \epsilon_2}{\epsilon_1 + \epsilon_2}$ . Also,

$$\begin{aligned} \varphi(y, 0) &= \int_0^\infty K(y, y') \rho(y') dy' \equiv \varphi(y), \\ K(y, y') &= \sum_{n=0}^\infty \frac{\xi^n}{2\pi\epsilon_0(\epsilon_1 + \epsilon_2)} \ln \frac{(y' - y)^2 + 4(n+1)^2 d^2}{(y' - y)^2 + (2nd)^2}. \end{aligned} \quad (3)$$

The electric field  $\mathcal{E}_z$  just above graphene ( $z = 0+$ ) is

$$\begin{aligned} \mathcal{E}_z(y) &\equiv -\partial_z \varphi(y, z)|_{z=0+} = \int_0^\infty K_{\mathcal{E}}(y, y') \rho(y') dy', \\ K_{\mathcal{E}}(y, y') &= \sum_{n=0}^\infty \frac{\xi^n d^2}{2\pi\epsilon_0(\epsilon_1 + \epsilon_2)} \left[ \frac{4n}{4(nd)^2 + (y - y')^2} \right. \\ &\quad \left. + \frac{4(n+1)}{4(n+1)^2 d^2 + (y - y')^2} \right]. \end{aligned}$$

The condition for electrochemical equilibrium for the composite system of graphene and donors is,

$$\varphi(y) + \frac{\rho(y) - \rho(\infty)}{e^2 \gamma} = -V_g, \quad (4)$$

and this leads to an inverse problem to find the charge density for a given voltage  $V_g$ .

Analytical solutions of Eqs. (3) and (4) are known for  $\gamma \rightarrow \infty$  in several asymptotic limits:

(a) For  $\epsilon_1 \rightarrow \infty$ , the substrate acts as a metal along the whole plane and the exact solution is  $\rho = \text{const}$ , corresponding to infinite plane capacitor.

(b) For finite  $\epsilon_{1,2}$ , the solution to Eqs. (3) and (4) has a singular behavior<sup>19,44,45</sup> near the edge of graphene,

$$\rho(y) \sim \mathcal{E}_z(y) \sim y^{-1/2}, \text{ for } \tilde{\gamma}^{-2} < \frac{y}{d} < 1,$$

while a finite density of states regularizes the divergence at  $y < d/\tilde{\gamma}^2$ , and the presence of a metallic top-gate is responsible for a stronger decay at  $y \gg d$ .

(c) When  $\epsilon_1 = \epsilon_2 = \epsilon$  ( $\xi = 0$  in Eq. (2)), the problem is reduced to finding the charge distribution near the ends of a plane capacitor<sup>44,46</sup>. A holomorphic mapping of infinite strip,  $(-V_g \leq \varphi \leq V_g, u)$ , to the complex  $y - z$  plane with two cuts,  $(y > 0, z = 0)$  and  $(y > 0, z = 2d)$ , produces a solution for potential  $\varphi$ ,

$$y + i(d - z) = -\frac{d}{\pi} \left[ e^{\frac{\pi}{V_g}(i\varphi + u)} + \frac{\pi}{V} (i\varphi + u) + 1 \right].$$

Exactly on graphene ( $z = 0$ ,  $\varphi = -V_g$ ), the auxiliary variable  $u$  is related to  $y$  via

$$\frac{\pi y}{d} = e^{\frac{\pi u}{V_g}} - \frac{\pi u}{V_g} - 1$$

with  $u < 0$  ( $u > 0$ ) corresponding to points just above (below) graphene (i.e.  $z = \pm 0$ ). Electric field near graphene is  $\mathcal{E}_z = \frac{V_g}{d} \frac{1}{1 - e^{\frac{\pi u}{V_g}}}$  and the charge density at  $z = 0$  is given by

$$\rho(y) = \frac{\mathcal{E}_z(y, +0) - \mathcal{E}_z(y, -0)}{\epsilon\epsilon_0} \underset{y \gg d}{\approx} \frac{V_g}{\epsilon_0 \epsilon d} \left( 1 + \frac{d}{\pi y} \right).$$

(d) For  $\epsilon_1 \ll \epsilon_2$ , one can find<sup>45</sup> for the electrostatic problem:

$$\rho(y) = \frac{-\epsilon_0 \epsilon_1 V_g}{d \sqrt{1 - e^{-\frac{\pi y}{d}}}}.$$

Aiming at modelling the devices used in the experiments reported in Refs.[34-36], we solve Eqs. (3) and (4) numerically for  $\tilde{\gamma} \gg 1$ . Then, knowing the form of all of

the above-listed asymptotics, we find the interpolation formula,

$$\rho(y) = \frac{-3.5V_g\epsilon_0}{d} \left( \frac{1}{\frac{1}{2\bar{\gamma}} + \sqrt{1 - e^{-\frac{\pi y}{2d}}} + \frac{0.5}{\frac{1}{\bar{\gamma}} + \sqrt{\frac{y}{d}}} \right),$$

$$\mathcal{E}_z(y) = \frac{-V_g}{d} \left( 1 + \frac{0.22e^{-\frac{2.5y}{d}}}{\frac{1}{\bar{\gamma}} + \sqrt{\frac{y}{d}}} \right), \quad (5)$$

which work with 1% accuracy for the obtained numerical solution.

### III. COMPRESSIBILITY OF QHE EDGE STATES IN G/SIC

Having found the total charge density of graphene electrons and SiC surface donors, we find how the total charge,  $\rho$ , is divided between graphene,  $-en_G$ , and SiC donor states,  $en_D$ . We relate the electrostatic potential for surface states in SiC,  $U_{SiC}$ , to electrostatic potential energy  $U$  of electrons in graphene as:

$$U_{SiC}(y) = U(y) - ed_1 \left[ \epsilon_2 \mathcal{E}_z(y) + \frac{en_G(y)}{\epsilon_0} \right]. \quad (6)$$

Here  $n_G(y)$  is the local electron density in graphene at point  $y$  and the density of donors on SiC surface is<sup>32,33,37</sup>:

$$n_{D+} = \gamma [A + U_{SiC}(y) - \mu], \quad (7)$$

where  $A \approx 0.2$  eV is a work function difference between charge-neutral SiC surface and undoped graphene. Electrochemical equilibrium conditions require that electrons in localized surface states on SiC have the same electrochemical potential,  $\mu$ , as graphene, which we count from the Dirac point in graphene far away from the edge, so that

$$\frac{n_G(y)}{\gamma_{\text{eff}}} = A - \mu + U(y) - e\epsilon_2 \mathcal{E}_z(y) d_1 - \frac{\rho(y)}{e\gamma}, \quad (8)$$

$$\frac{1}{\gamma_{\text{eff}}} \equiv \frac{1}{\gamma} + \frac{d_1 e^2}{\epsilon_0}.$$

In general, the relation between  $U(y)$  and  $n_G(y)$  is non-local [see Eq. (12) below]. However, in the case that potential  $U(y)$  varies slowly at the length scale of magnetic length,  $l_B = \sqrt{\frac{\hbar}{eB}}$ , ( $\nabla U \ll \frac{\hbar v}{l_B^2}$ ), one may approximate

$$\mu - U(y) = -\frac{1}{\gamma_{\text{eff}}} \frac{1}{\pi l_B^2} \int dy_0 \left[ \sum_{n=-N}^N |\psi_{n,y_0}(y)|^2 \text{Erf} \frac{\int |\psi_{n,y_0}(y)|^2 (\mu - U(y) - E_n) dy}{\Delta} \right] + A - \frac{\rho(y)}{e\gamma} - e\epsilon_2 \mathcal{E}_z(y) d_1. \quad (12)$$

The latter equation can be solved iteratively<sup>47</sup>. The re-

sults of numerical solution of Eq. (12) are shown in Fig.

$$E_n + U(y) = \frac{\hbar v}{l_B} \text{sign}(n) \sqrt{2|n|} + U(y). \quad (9)$$

the local energy of Landau levels (LL) in graphene as

The local density of electrons can be related to the local filling factor,  $\nu_n(y)$ , determined by the number of filled LLs and spin/valley degeneracy,

$$n_G(y) \approx \frac{eB}{h} \nu(y). \quad (10)$$

Solving Eq. (8) with  $n_G$  given above leads to results shown by dotted lines in Fig. 2. The resulting potential on graphene have a number of horizontal intervals, which would correspond to compressible stripes, if the conditions for validity of quasiclassical approximations are satisfied.

When the width of a stripe is comparable to magnetic length,  $l_B$ , we must account for a finite extent of electron's wave functions in a magnetic field, therefore, going beyond the quasi-classical approximation used in Eq. (10). Here, we use Landau gauge and parameterise states with momentum  $p$  along the edge, related to the distance of electronic wave function from the edge,  $y_0 = -l_B^2 p$ . When  $y_0 \gtrsim 2l_B$ , wave functions of LLs have a Gaussian form:

$$|\psi_{0,y_0}(y)|^2 = \frac{1}{\sqrt{\pi} l_B} e^{-\delta^2}, \quad \delta \equiv \frac{y - y_0}{l_B};$$

$$|\psi_{n \neq 0, y_0}(y)|^2 = \frac{H_{|n|}^2(\delta) + 2|n| H_{|n|-1}^2(\delta)}{2^{|n|+1} |n|! \sqrt{\pi} l_B} e^{-\delta^2},$$

where  $H_n(x)$  are Hermite polynomials. While for a smooth potential  $U(y)$ ,  $E_{n,y_0} \approx E_n + U(y_0)$ , but, due to potential having cusp-like features near the ends of compressible stripes (see Fig. 2), we use a more precise expression for the LL energy and electron density in graphene,

$$E_{n,y_0} \approx \int |\psi_{n,y_0}(y)|^2 U(y) dy, \quad (11)$$

$$n_G(y) = \frac{1}{2\pi l_B^2} \sum_{n=-N}^N \int |\psi_{n,y_0}(y)|^2 \tilde{\nu}_n(y_0) dy_0,$$

$$\tilde{\nu}_n(y_0) \equiv 2 \text{Erf} \frac{\int |\psi_{n,y_0}(y)|^2 [\mu - U(y) - E_n] dy}{\Delta},$$

where we introduced a small Gaussian LL broadening,  $\Delta$ , and a LL cut-off,  $N$ , for the convergence of our numerical procedure. Note that the result is independent of  $N$  when  $|\mu - U(y)| \leq \frac{\hbar v}{l_B} \sqrt{2N}$ . Together with Eq. (8), Eq. (12) results in a non-linear integral equation for  $U(y)$ ,

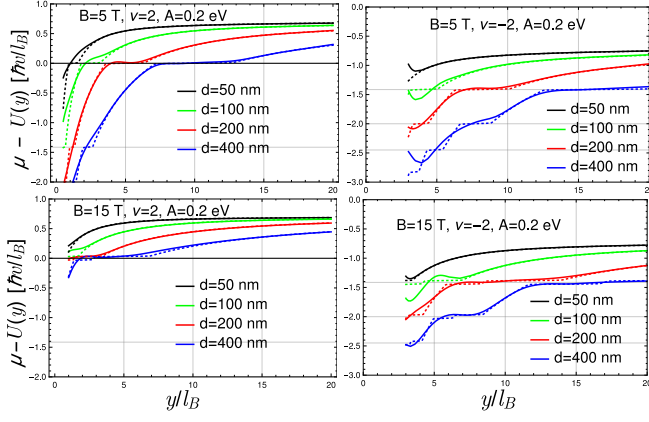


FIG. 2. Self-consistent electrostatic potential induced in G/SiC for  $B = 5$  T and  $B = 15$  T, bulk filling factor  $\nu = \pm 2$  (left/right columns)  $d = 50, 100, 200, 400$  nm (top to bottom). Fermi level is chosen as  $\mu = \pm \frac{1}{\sqrt{2}} \frac{\hbar v}{l_B}$ , corresponding to the middle of the gap for  $\nu = \pm 2$ . Dashed line corresponds to quasi-classical calculation, Eq. (10); solid lines are self-consistent calculation, Eq. (12). For  $B = 15$  T, we illustrate the effect of interaction-induced level splitting by 6 meV.

2, where flat intervals of potential (precursors of compressible stripes) are formed: those are about  $\sim l_B$  (or  $\sim 2l_B$  for  $\nu = -2$ ) narrower than what was expected from the quasi-classical estimations. Note that the non-locality in Eq. (12) arises due to a finite ( $|y - y_0| \sim l_B$ ) extent of the wave function, rather than long-range Coulomb interactions (as it would be in a 2DEG in GaAs/AlGaAs<sup>9,15–18</sup> or in a GraFET, Section IV). We note a significant particle-hole ( $\nu = \pm 2$ ) asymmetry of the potential profile that is caused by a significant initial n-doping of G/SiC: the gate potential has the same sign for both  $\nu = +2$  and  $\nu = -2$  but it is stronger for  $\nu = -2$ .

Also, at distances  $\sim l_B$  near the edge, the electronic wave functions do not have Gaussian shape, but this can be incorporated in the change of boundary conditions for Dirac electrons, as discussed below<sup>50</sup>. Generic boundary conditions<sup>14,51,52</sup> for graphene electrons near the edge are:

$$\begin{aligned} v\boldsymbol{\sigma} \cdot (-i\hbar\nabla + e\mathbf{A})\Psi &= (E - U(y))\Psi; \\ [1 - (\mathbf{m} \cdot \boldsymbol{\tau}) \otimes (\mathbf{n} \cdot \boldsymbol{\sigma})]\Psi|_{y=0} &= 0; \\ \mathbf{n} &= \hat{\mathbf{n}}_z \cos \phi + [\hat{\mathbf{n}}_z \times \mathbf{n}_\perp] \sin \phi. \end{aligned} \quad (13)$$

Here,  $\sigma_i$  and  $\tau_i$  are Pauli matrices acting separately on sublattice ( $A, B$ ) and valley ( $\pm K$ ) components of a 4-spinor,  $\Psi^T = (\Psi_{KA}, \Psi_{KB}, \Psi_{-KB}, -\Psi_{-KA})$ , describing the electron amplitudes on sublattices  $A$  and  $B$  in the valleys  $\pm K$ . Coordinate axes here are the same as in electrostatics analysis: electrons move freely in half-plane:  $-\infty < x < \infty, y > 0, z = 0$  with the straight edge ( $x, y = 0, z = 0$ ). Generic boundary conditions<sup>14,51,52</sup> in Eq. (13) are parameterized by two unit vectors,  $\mathbf{m}$  and  $\mathbf{n} \perp \mathbf{n}_\perp$ , where  $\mathbf{n}_\perp$  is normal to the edge and lays within the 2D plane of graphene. Both  $\mathbf{m}$  and  $\mathbf{n}$  depend on the microscopic features of the edge in a particular sample.

A rotation of multi-spinor  $\Psi$  in the valley space can be used<sup>14</sup> to set  $\mathbf{m} = \hat{\mathbf{n}}_z$ , so that angle  $\phi$  (corresponding to the direction of vector  $\mathbf{n}_\perp$ ) is the only relevant boundary parameter ( $\phi \in [0, \pi]$  and  $\phi \rightarrow \phi + \pi$  is obtained by swapping the valleys).

For calculating edge states, we use Landau gauge for vector potential,  $\mathbf{A} = (By, 0)$ , and characterise states by wave-number  $p$  along the edge,  $\Psi(x, y) = e^{ipx}\psi(y)$ . Typical dispersions  $E(p)$  are shown in Fig. 3. These spectra are valley-degenerate away from the edge, while at distances  $y \lesssim 2l_B$  ( $-pl_B < 2$ ) the valley degeneracy is broken. When the top gate is close to graphene, e.g.  $d \lesssim 50$  nm, the spectrum is qualitatively similar to the case of zero potential<sup>14,25–29</sup>, though with some renormalization of  $\phi$ , caused by potential variation at short distances ( $y \lesssim l_B$ ) near the edge: we find<sup>50</sup> that  $\phi$  is effectively increased (decreased) by a positive (negative) peak of potential near the edge of graphene. For such close gates, there is only one edge channel (per spin) with chirality prescribed by the bulk filling factor ( $\nu = 2$ , or  $\nu = -2$ ). For  $d \gtrsim 100$  nm, the first pair of counter-propagating edge channels starts to appear, as pointed in Fig. 3 by an arrow. We find that for  $d \gtrsim 20l_B$  ( $d > 200$  nm in Fig. 3) the edge channel starts to develop a narrow valley-degenerate compressible stripe.

Besides the above-listed features, common for  $\nu = 2$  and  $\nu = -2$ , there are the following notable differences between those two filling factors. First of all, extra pairs of edge states and compressible stripes correspond to the 0-th LL for  $\nu = 2$  and to the “ $n = -1$ ” LL for  $\nu = -2$ . Then, apart from the expected continuation of the bulk Landau levels, we observe extra branches of evanescent edge modes that generalize the zigzag edge modes<sup>25–29</sup> to generic boundary conditions. For  $\nu = 2$ , there is only one such branch in each of the valleys, with its dispersion depending on the renormalized value of  $\phi$ . It approaches the Fermi level at low values of  $p l_B$ , resulting in strong mixing with LL branches and multiple avoided crossings. In G/SiC reaching  $\nu = -2$  requires larger top-gate voltage, making the effects of external potential stronger. This is reflected in more evanescent modes, that cross Fermi level at larger values of  $|p l_B|$ . Note that these edge modes are present even in a zero magnetic field and may be explained by full internal reflection from the potential wall<sup>48,49</sup>.

#### IV. COMPRESSIBILITY OF QHE EDGE STATES IN GraFETs

For comparison, in GraFETs, graphene doping is provided solely by electrons transferred from the gate. In this case, we solve a self-consistent nonlinear integral equation<sup>9,15–18</sup>, describing potential near GraFET edge,

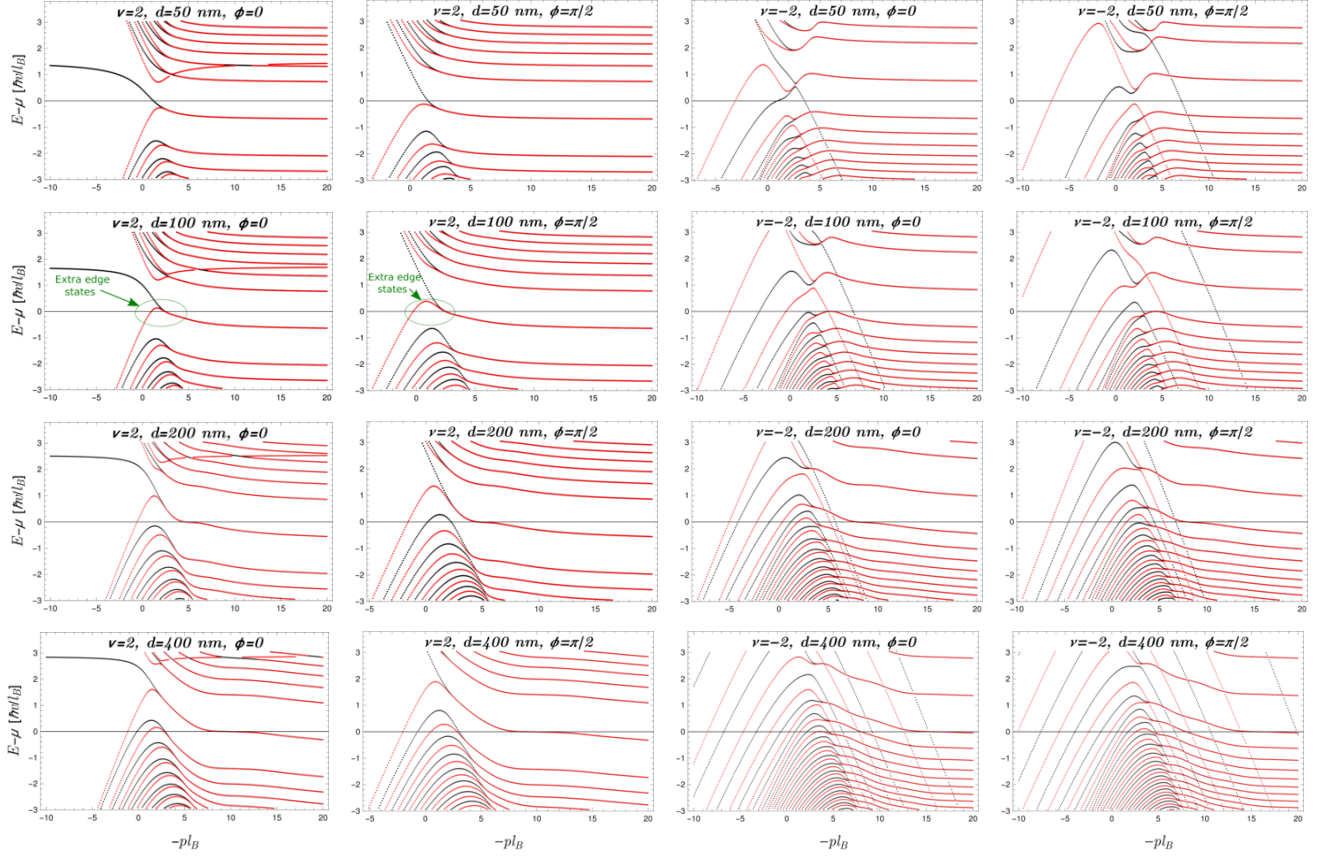


FIG. 3. Electronic spectrum in magnetic field  $B = 5$  T calculated for two examples of boundary conditions:  $\phi = 0$  and  $\phi = \pi/2$  and for filling factors  $\nu = \pm 2$ . Edge states correspond to levels crossing the Fermi-level, compressible stripes correspond to flat intervals of dispersion at  $E = \mu$ . Black/red color corresponds to different  $\pm K$  valleys. Extra branches for  $\nu = -2$  are the evanescent waves, localized in the area of large potential near the edge (similar to “whispering gallery” modes in Ref. 48 and 49).

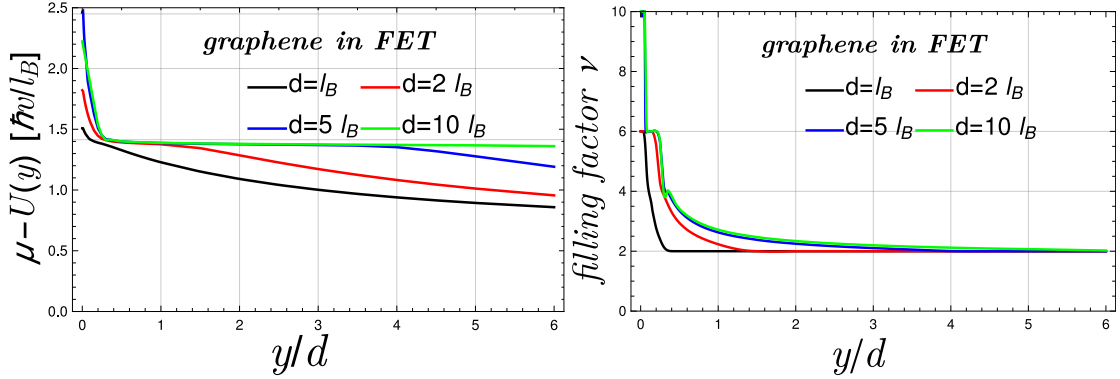


FIG. 4. Self-consistent potential (local Fermi energy),  $\mu - U(y)$ , and the filling factor,  $\nu$ , in GraFET. Top gate voltage  $V_g$  is tuned to achieve a midgap chemical potential in the center of a device, chosen to have a width  $50d$ . Long-range Coulomb interaction leads to wide compressible stripes (corresponding to LL with  $n = 1$ ) developing already for  $d \gtrsim 2l_B$ .

$$U(y) = \frac{\hbar v}{l_B} \kappa \int_0^\infty \frac{dy'}{d} \nu(y') \sum_{n=0}^\infty \xi^n \ln \frac{(y' - y)^2 + 4(n+1)^2 d^2}{(y' - y)^2 + (2nd)^2}, \quad (14)$$

with  $\kappa = \frac{e^2}{(2\pi)^2 \hbar v \epsilon_0 (\epsilon_1 + \epsilon_2)} \frac{d}{l_B} \approx 0.05 \frac{d}{l_B}$  (we use  $\epsilon_1 = 9.7$ ,  $\epsilon_2 = 3.5$ ) and  $\nu(y) = \sum_{n=-N}^N 2 \text{Erf} \frac{\mu - U(y) - E_n}{\Delta}$ . The nonlocality in it is produced by the long-range nature of Coulomb potential, so that the “edge-of-capacitor” effect extends over longer distances, as compared to G/SiC system. This supports the use of quasi-classical approxi-

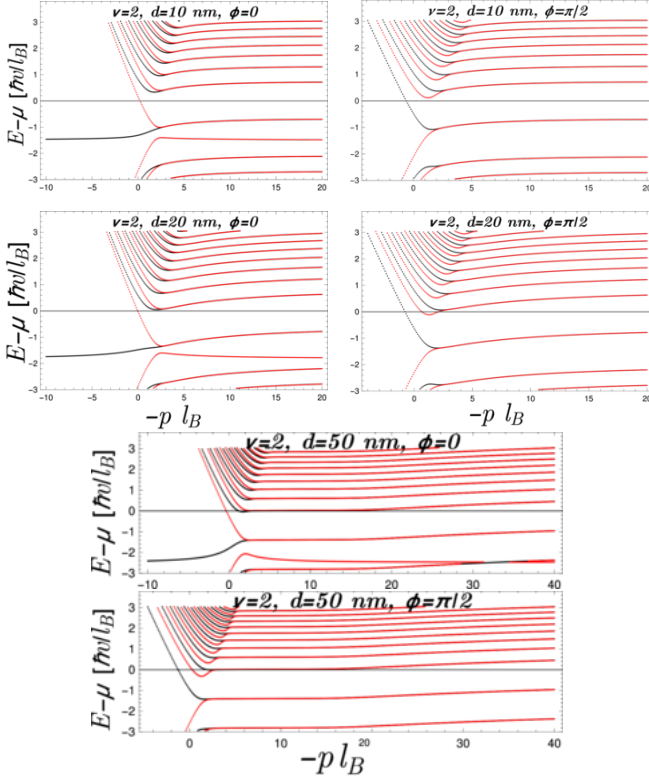


FIG. 5. Edge state dispersion in GraFET with boundary condition parameters  $\phi = 0$  and  $\phi = \pi/2$ , for  $B = 5$  T. Black/red color corresponds to different  $\pm K$  valleys. Compressible stripe starts to develop already for  $d > 2l_B \approx 20$  nm, getting  $\mathcal{L} \sim 20l_B$  wide at  $d = 5l_B$  and rapidly growing further with increasing  $d$ . For  $\phi = 0$  note the appearance of an almost flat branch of evanescent edge modes below the Fermi level.

mation,  $2\pi l_B^2 n_G(y) = \nu(y)$ , which is then justified by the results, Figs. 4 and 5, showing compressible stripes with widths  $\mathcal{L} \gg l_B$  that appear at  $y \gg l_B$ .

Choosing the top-gate voltage,

$$eV_g = \frac{\hbar v}{l_B} \left[ 2\kappa \frac{2\pi(\epsilon_1 + \epsilon_2)}{\epsilon_2} + \frac{1}{\sqrt{2}} \right],$$

to get  $\nu = 2$  away from the boundary<sup>53</sup>, we solve Eq. (14) numerically. For numerical simulations<sup>47</sup>, we set width of  $50d$  for the modeled GraFET device and tune chemical potential to the middle of the gap in the center of the device. The results of numerical simulations are shown in Fig. 4 and the LL spectrum is plotted in Fig. 5. Results for  $\nu = -2$  can be obtained by reversing the sign of energy and changing<sup>14</sup>  $\phi \rightarrow -\phi$ . As compared to the case of G/SiC, the opposite (positive) sign of top gate voltage is needed to dope graphene to the filling factor  $\nu = 2$ , which leads to a stronger electron doping near the edge. As a result, for increasing  $d$ , extra counter-propagating edge channels correspond to filling of the 1-st LL, in contrast to the 0-th LL in case of  $\nu = 2$  in G/SiC. Another difference is that the inner edge channel reconstructs easier into a wide compressible stripe (now, for the 1-st LL).

This starts to happen already at  $d \sim 2l_B$ , and the compressible stripe rapidly grows upon increasing  $d$ , see Figs. 4 and 5. This latter remark can be used to interpret the recent experiment<sup>20</sup>, where the formation of a wide compressible stripe has prevented the edge metallization contacts from measuring the  $\nu = 2$  resistance plateau, despite the  $\nu = 2$  incompressible state in the bulk of the sample.

## V. DISCUSSIONS AND CONCLUSIONS

The analysis of the electrostatics of QHE edge states in graphene presented in Sections II - IV establishes that formation of compressible stripes near the edge is suppressed in G/SiC, as compared to GraFETs and 2DEG in GaAs/AlGaAs heterostructures. Numerical solutions of Eqs. (12) and (14) for the potential and Eq. (13) for the spectrum allows us to calculate the width,  $\Delta p$ , of flat interval in the dispersion at the Fermi level (where  $E(p) = \mu$ ). The corresponding states are located at  $y \approx -pl_B^2$  thus forming a compressible stripe of width  $\mathcal{L} = l_B^2 \Delta p$ . To illustrate the result quantitatively, we choose the device parameters that provide  $\nu = \pm 2$  QHE plateaux for  $B = 5$  Tesla and  $B = 15$  Tesla, motivated by the implementation of G/SiC in the primary<sup>34</sup> (15 Tesla range) and a “push-button”<sup>35</sup> (5 Tesla range) quantum resistance standards by National Physical Laboratory (UK) and Oxford Instruments PLC.

The results for the compressible stripe length,  $\mathcal{L}$ , are gathered in Fig.6 from both G/SiC and GraFETs. They highlight an essential feature of G/SiC determined by the presence of surface states in the “dead layer” of SiC surface, which leads to significant electron doping of graphene (so that the opposite signs of gate potentials are needed to achieve  $\nu = 2$  in G/SiC and in GraFETs) and to an efficient electrostatic screening. As a result, compressible stripes in G/SiC are possible only for distances  $d \gtrsim 20l_B$  between graphene and the gate, and even then their widths,  $\mathcal{L}$ , are order of magnitude smaller than in GraFETs, Fig. 6. Semiclassically, one would estimate<sup>16,45</sup>  $\mathcal{L}$  as a distance at which the filling factor changes by 4, which would give a linear dependence for G/SiC<sup>54</sup>,

$$\mathcal{L} \approx \frac{4eB}{h\gamma_{\text{eff}} \left| \frac{\partial_y \rho(y)}{e\gamma} + \partial_y \mathcal{E}_z(y) e\epsilon_2 d_1 \right|} \Bigg|_{y=y_c, U(y_c)=\mu} \propto d.$$

Note that by the definition in Eq. (8),  $\gamma_{\text{eff}} < \epsilon_0 d_1 / e^2$ , whereas would it be formally set to  $\gamma_{\text{eff}} \rightarrow \infty$ , no compressible stripe could form. Also, magnetic field dependence of  $\mathcal{L}$  is different from linear, because at fixed filling factor in the 2D bulk, changing magnetic field would be accompanied by changing gate voltage (hence,  $\mathcal{E}_z$  and  $\rho$  are changing). For example, at large magnetic fields ( $B \sim 20$  T), no gate voltage is needed to get  $\nu = 2$

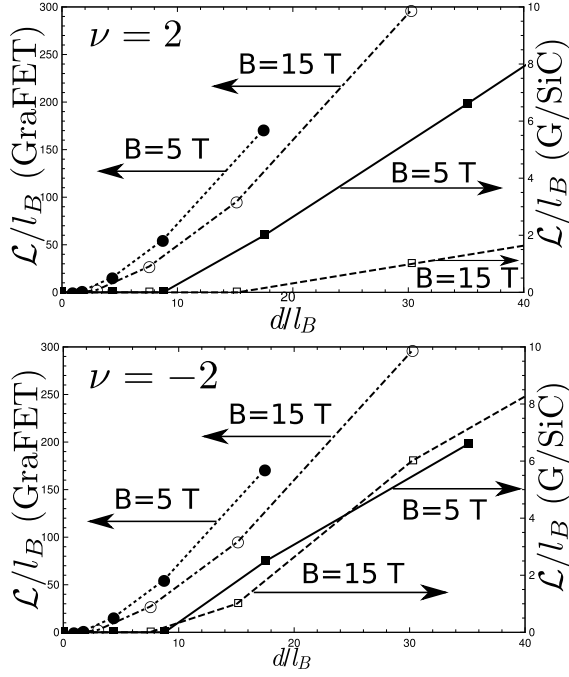


FIG. 6. Compressible stripe width,  $\mathcal{L}$ , near the  $\nu = \pm 2$  QHE edge in graphene in G/SiC (squares) and GraFET (circles) as a function of a distance to the top gate,  $d$ , for  $B = 5$  T (filled symbols) and  $B = 15$  T (open symbols). Note the difference between r.h.s. and l.h.s. axes, stressing the fact that compressible stripes in GraFETs are much wider than in G/SiC.

in the bulk and no compressible stripes are expected, while for  $\nu = -2$  the needed gate voltage increases

with magnetic field, which may lead to wider compressible stripe at larger  $B$ . The above quasichlassical estimate agrees with the results shown in Fig. 6 upon subtraction of  $\sim 2l_B$  for  $\nu = 2$  and  $\sim 4l_B$  for  $\nu = -2$ , which accounts for a finite extent,  $\sim l_B$ , of electron wave functions in the relevant LLs. The latter difference is one of the manifestations of the “electron-hole” asymmetry of QHE edge states in G/SiC, in contrast to “e-h” ( $\nu \rightarrow -\nu$ ) symmetry of QHE edge states in GraFETs. This “e-h” asymmetry of G/SiC is determined by that reverting graphene doping from n-type ( $\nu = 2$ ) to p-type ( $\nu = -2$ ) requires further increasing gate voltage rather than reverting the sign of gate voltage as in the case of GraFET. The resulting potential inhomogeneity near the edge is stronger for  $\nu = -2$  in G/SiC, leading to a larger number of counter-propagating pairs of evanescent edge modes that are present even at zero magnetic field<sup>48,49</sup>. Counter-propagating modes lead to dissipative QHE<sup>55</sup> unless they are not gapped by 1D localization, induced by inter-channel scattering.

A sharper potential near the edge and narrower (or fully suppressed) compressible stripes in G/SiC would make equilibration<sup>7,10,11,56</sup> of edge channels faster than in GraFETs with similar parameters. At the same time, cooling of edge state electrons by phonon emission<sup>14</sup> would be slower in G/SiC, with hot electrons spreading to longer distances along the edge.

*Acknowledgements* We acknowledge useful discussions with K. von Klitzing, S. Rozhko, A. Tzalenchuk, J.T. Janssen, R. Nicholas, F. Essler, J. Wallbank, M. Ben Shalom and constructive remarks of the Referees. This work was funded by Innovate UK grant 65431-468182 and the European Graphene Flagship project.

\* on leave of absence from NRC “Kurchatov Institute” PNPI, Russia.  
<sup>1</sup> K. V. Klitzing, G. Dorda, and M. Pepper, Phys. Rev. Lett. **45**, 494 (1980).  
<sup>2</sup> R. B. Laughlin, Phys. Rev. B **23**, 5632 (1981).  
<sup>3</sup> Q. Niu, D. J. Thouless, and Y.-S. Wu, Phys. Rev. B **31**, 3372 (1985).  
<sup>4</sup> Q. Niu and D. J. Thouless, Phys. Rev. B **35**, 2188 (1987).  
<sup>5</sup> M. Büttiker, Phys. Rev. B **38**, 9375 (1988).  
<sup>6</sup> K. von Klitzing, Rev. Mod. Phys. **58**, 519 (1986).  
<sup>7</sup> B. W. Alphenaar, P. L. McEuen, R. G. Wheeler, and R. N. Sacks, Phys. Rev. Lett. **64**, 677 (1990).  
<sup>8</sup> T. Martin and S. Feng, Phys. Rev. Lett. **64**, 1971 (1990).  
<sup>9</sup> K. Güven and R. R. Gerhardt, Phys. Rev. B **67**, 115327 (2003).  
<sup>10</sup> D.-K. Ki and H.-J. Lee, Phys. Rev. B **79**, 195327 (2009).  
<sup>11</sup> D. L. Kovrizhin and J. T. Chalker, Phys. Rev. B **84**, 085105 (2011).  
<sup>12</sup> G. Granger, J. P. Eisenstein, and J. L. Reno, Phys. Rev. Lett. **102**, 086803 (2009).  
<sup>13</sup> S.-G. Nam, E. H. Hwang, and H.-J. Lee, Phys. Rev. Lett. **110**, 226801 (2013).  
<sup>14</sup> S. Slizovskiy and V. Fal’ko, Phys. Rev. B **96**, 075434

(2017).  
<sup>15</sup> U. Wulf, V. Gudmundsson, and R. R. Gerhardt, Phys. Rev. B **38**, 4218 (1988).  
<sup>16</sup> D. B. Chklovskii, B. I. Shklovskii, and L. I. Glazman, Phys. Rev. B **46**, 4026 (1992).  
<sup>17</sup> N. R. Cooper and J. T. Chalker, Phys. Rev. B **48**, 4530 (1993).  
<sup>18</sup> M. M. Fogler, E. I. Levin, and B. I. Shklovskii, Phys. Rev. B **49**, 13767 (1994).  
<sup>19</sup> P. G. Silvestrov and K. B. Efetov, Phys. Rev. B **77**, 155436 (2008).  
<sup>20</sup> Y.-T. Cui, B. Wen, E. Y. Ma, G. Diankov, Z. Han, F. Amet, T. Taniguchi, K. Watanabe, D. Goldhaber-Gordon, C. R. Dean, and Z.-X. Shen, Phys. Rev. Lett. **117**, 186601 (2016).  
<sup>21</sup> I. J. Vera-Marun, P. J. Zomer, A. Veligura, M. H. D. Guimares, L. Visser, N. Tombros, H. J. van Elferen, U. Zeitler, and B. J. van Wees, Applied Physics Letters **102**, 013106 (2013).  
<sup>22</sup> S. Ihnatsenka and I. V. Zozoulenko, Phys. Rev. B **86**, 155407 (2012).  
<sup>23</sup> A. A. Shylau, I. V. Zozoulenko, H. Xu, and T. Heinzel, Phys. Rev. B **82**, 121410 (2010).

- <sup>24</sup> In contrast to 2DEG created by smooth gate potentials, graphene has a finite density of states up to the very edge of the flake. This leads to a singularity in the charge density near the edge, known to appear in thin charged metal plates<sup>44</sup>.
- <sup>25</sup> N. M. R. Peres, F. Guinea, and A. H. Castro Neto, Phys. Rev. B **73**, 125411 (2006).
- <sup>26</sup> D. A. Abanin, P. A. Lee, and L. S. Levitov, Phys. Rev. Lett. **96**, 176803 (2006).
- <sup>27</sup> D. A. Abanin, P. A. Lee, and L. S. Levitov, Solid State Commun. **143**, 77 (2007).
- <sup>28</sup> L. Brey and H. A. Fertig, Phys. Rev. B **73**, 195408 (2006).
- <sup>29</sup> G. Li, A. Luican-Mayer, D. Abanin, L. Levitov, and E. Y. Andrei, Nature Communications **4**, 1744 (2013).
- <sup>30</sup> H. Tetlow, J. P. de Boer, I. Ford, D. Vvedensky, J. Coraux, and L. Kantorovich, Physics Reports **542**, 195 (2014), growth of epitaxial graphene: Theory and experiment.
- <sup>31</sup> A. Bostwick, J. McChesney, T. Ohta, E. Rotenberg, T. Seyller, and K. Horn, Progress in Surface Science **84**, 380 (2009).
- <sup>32</sup> S. Kopylov, A. Tzalenchuk, S. Kubatkin, and V. I. Fal'ko, Applied Physics Letters **97**, 112109 (2010).
- <sup>33</sup> A. Tzalenchuk, S. Lara-Avila, A. Kalaboukhov, S. Paolillo, M. Syväjärvi, R. Yakimova, O. Kazakova, T. J. B. M. Janssen, V. Fal'ko, and S. Kubatkin, Nature Nanotechnology **5**, 186 (2010).
- <sup>34</sup> T. J. B. M. Janssen, A. Tzalenchuk, S. Lara-Avila, S. Kubatkin, and V. I. Fal'ko, Rep. Prog. Phys. **76**, 104501 (2013).
- <sup>35</sup> T. J. B. M. Janssen, S. Rozhko, I. Antonov, A. Tzalenchuk, J. M. Williams, Z. Melhem, H. He, S. Lara-Avila, S. Kubatkin, and R. Yakimova, 2D Materials **2**, 035015 (2015).
- <sup>36</sup> J. A. Alexander-Webber, J. Huang, D. K. Maude, T. J. B. M. Janssen, A. Tzalenchuk, V. Antonov, T. Yager, S. Lara-Avila, S. Kubatkin, R. Yakimova, and R. J. Nicholas, Scientific Reports **6**, 30296 (2016).
- <sup>37</sup> T. J. B. M. Janssen, A. Tzalenchuk, R. Yakimova, S. Kubatkin, S. Lara-Avila, S. Kopylov, and V. I. Fal'ko, Phys. Rev. B **83**, 233402 (2011).
- <sup>38</sup> M. Woszczyzna, M. Friedemann, M. Gtz, E. Pesel, K. Pierz, T. Weimann, and F. J. Ahlers, Appl. Phys. Lett. **100**, 164106 (2012).
- <sup>39</sup> F. Lafont, R. Ribeiro-Palau, D. Kazazis, A. Michon, O. Couturaud, C. Consejo, T. Chassagne, M. Zielinski, M. Portail, B. Jouault, F. Schopfer, and W. Poirier, Nature Communications **6**, 6806 (2015).
- <sup>40</sup> M. Yang, O. Couturaud, W. Desrat, C. Consejo, D. Kazazis, R. Yakimova, M. Syväjärvi, M. Goiran, J. Béard, P. Frings, M. Pierre, A. Cresti, W. Escoffier, and B. Jouault, Phys. Rev. Lett. **117**, 237702 (2016).
- <sup>41</sup> T. Shen, W. Wu, Q. Yu, C. A. Richter, R. Elmquist, D. Newell, and Y. P. Chen, Appl. Phys. Lett. **99**, 232110 (2011).
- <sup>42</sup> F. D. Parmentier, T. Cazimajou, Y. Sekine, H. Hibino, H. Irie, D. C. Glatli, N. Kumada, and P. Rouleau, Scientific Reports **6**, 38393 (2016).
- <sup>43</sup> S. Lara-Avila, K. Moth-Poulsen, R. Yakimova, T. Bjrnholm, V. Falko, A. Tzalenchuk, and S. Kubatkin, Adv. Mater. **23**, 878 (2011).
- <sup>44</sup> J. D. Johnson, *Classical electrodynamics* (John Wiley & Sons, Inc., 1962).
- <sup>45</sup> A. V. Khaetskii, V. I. Fal'ko, and G. E. W. Bauer, Phys. Rev. B **50**, 4571 (1994).
- <sup>46</sup> M. A. Lavrentiev and B. V. Shabat, *Metodi teorii funktsii kompleksnogo peremennogo (Methods of theory of complex variable)* (Moscow, Nauka, 1974).
- <sup>47</sup> The function  $U(y)$  is interpolated with  $\sim 50$  points and iterations are done as  $U_{new} = \alpha U(U_{old}) + (1-\alpha)U_{old}$  with a factor  $\alpha \leq 1$  small enough to reach convergence. At small  $\Delta$  the non-linearity gets strong and we need to choose rather small values  $\alpha \sim 0.001$  to achieve convergence.
- <sup>48</sup> V. V. Cheianov and V. I. Fal'ko, Phys. Rev. B **74**, 041403 (2006).
- <sup>49</sup> Y. Zhao, J. Wyrick, F. D. Natterer, J. F. Rodriguez-Nieva, C. Lewandowski, K. Watanabe, T. Taniguchi, L. S. Levitov, N. B. Zhitenev, and J. A. Stroscio, Science **348**, 672 (2015).
- <sup>50</sup> The boundary conditions can be used to incorporate the sample-dependent variations of potential near the edge of graphene, which arise due to chemical and electrostatic modification of the edge. To consider the effect of a large potential  $U(y)$  near the edge, let us start solving the Dirac equation from a point  $y_0 > 0$ , hence, we need a new boundary condition,  $\phi(y_0)$ . We find that Eq. (13) leads to
- $$\frac{d}{dy}\phi(y) = 2\frac{U(y) - E}{\hbar v} + 2\left(p + \frac{y}{l_B^2}\right) \pm \sin\phi(y),$$
- producing a flow of boundary conditions for valleys  $\pm K$  (we do not loose solutions in this procedure if the second, nonlinear, term can be neglected relative to the first term). This flow depends on valley,  $p$  and  $E$ , producing a more general class of  $E^-$  and  $p^-$  dependent boundary conditions. Considering the flow in the region of large  $|U|$  ( $|E| \ll |U(y)|$  for  $y < y_0$ ), and concentrating on low  $|p|$ , leads to an approximate equation  $\frac{d}{dy}\phi(y) \approx 2\frac{U(y)}{\hbar v}$ . It means that when  $U(y)$  is positive (negative) near the edge, the effective boundary parameter increases (decreases) as we move away from the edge. As a result, the sample-dependent details of the potential near the edge can be absorbed into a renormalization of  $\phi$ . For example, the standard zigzag boundary conditions,  $\phi(0) = 0$ , behave similarly to  $\phi \approx \pi/4$  in G/SiC at  $\nu = 2$ . Note that at large and wide potential near the edge (as happens for  $\nu = -2$  in our discussion), moving  $y_0$  to the safe region of low potential will involve  $\phi$  making several  $2\pi$  turns, resulting in the loss of several solutions, corresponding to extra evanescent modes<sup>48,49</sup>.
- <sup>51</sup> A. R. Akhmerov and C. W. J. Beenakker, Phys. Rev. B **77**, 085423 (2008).
- <sup>52</sup> E. McCann and V. I. Fal'ko, J. Phys., Condens. Mat. **16**, 2371 (2004).
- <sup>53</sup> This equation is easily derived from the plain capacitor geometry and the requirement  $\mu = \frac{\hbar v}{l_B} \frac{1}{\sqrt{2}}$ ,  $\rho = 2e/(2\pi l_B^2)$ .
- <sup>54</sup> To estimate  $\mathcal{L}$  we use Eq. (8). The dependence  $\mathcal{L} \propto d$  follows from the scaling  $\mathcal{E}_z(y; d) = \tilde{\mathcal{E}}_z(y/d)/d$  and  $\rho(y; d) = \tilde{\rho}(y/d)/d$  in Eq. (5).
- <sup>55</sup> D. A. Abanin, K. S. Novoselov, U. Zeitler, P. A. Lee, A. K. Geim, and L. S. Levitov, Phys. Rev. Lett. **98**, 196806 (2007).
- <sup>56</sup> F. Amet, J. R. Williams, K. Watanabe, T. Taniguchi, and D. Goldhaber-Gordon, Phys. Rev. Lett. **112**, 196601 (2014).